

Open Research Online

The Open University's repository of research publications and other research outputs

CO₂ drawdown following the middle Miocene expansion of the Antarctic Ice Sheet

Journal Item

How to cite:

Badger, Marcus P.S.; Lear, Caroline H.; Pancost, Richard D.; Foster, Gavin L.; Bailey, Trevor R.; Leng, Melanie J. and Abels, Hemmo A. (2013). CO₂ drawdown following the middle Miocene expansion of the Antarctic Ice Sheet. *Paleoceanography*, 28(1) pp. 42–53.

For guidance on citations see [FAQs](#).

© [\[not recorded\]](#)

Version: Version of Record

Link(s) to article on publisher's website:
<http://dx.doi.org/doi:10.1002/palo.20015>
<http://dx.doi.org/10.1002/palo.20015>

Copyright and Moral Rights for the articles on this site are retained by the individual authors and/or other copyright owners. For more information on Open Research Online's data [policy](#) on reuse of materials please consult the policies page.

oro.open.ac.uk

CO₂ drawdown following the middle Miocene expansion of the Antarctic Ice Sheet

Marcus P. S. Badger,^{1,2,3*} Caroline H. Lear,¹ Richard D. Pancost,² Gavin L. Foster,^{4,5} Trevor R. Bailey,⁶ Melanie J. Leng,⁷ and Hemmo A. Abels⁸

Received 27 July 2012; revised 18 January 2013; accepted 22 January 2013; published 22 March 2013.

[1] The development of a permanent, stable ice sheet in East Antarctica happened during the middle Miocene, about 14 million years (Myr) ago. The middle Miocene therefore represents one of the distinct phases of rapid change in the transition from the “greenhouse” of the early Eocene to the “icehouse” of the present day. Carbonate carbon isotope records of the period immediately following the main stage of ice sheet development reveal a major perturbation in the carbon system, represented by the positive $\delta^{13}\text{C}$ excursion known as carbon maximum 6 (“CM6”), which has traditionally been interpreted as reflecting increased burial of organic matter and atmospheric $p\text{CO}_2$ drawdown. More recently, it has been suggested that the $\delta^{13}\text{C}$ excursion records a negative feedback resulting from the reduction of silicate weathering and an increase in atmospheric $p\text{CO}_2$. Here we present high-resolution multi-proxy (alkenone carbon and foraminiferal boron isotope) records of atmospheric carbon dioxide and sea surface temperature across CM6. Similar to previously published records spanning this interval, our records document a world of generally low (~ 300 ppm) atmospheric $p\text{CO}_2$ at a time generally accepted to be much warmer than today. Crucially, they also reveal a $p\text{CO}_2$ decrease with associated cooling, which demonstrates that the carbon burial hypothesis for CM6 is feasible and could have acted as a positive feedback on global cooling.

Citation: Badger, M. P. S., C. H. Lear, R. D. Pancost, G. L. Foster, T. R. Bailey, M. J. Leng, and H. A. Abels (2013), CO₂ drawdown following the middle Miocene expansion of the Antarctic Ice Sheet, *Paleoceanography*, 28, 42–53, doi:10.1002/palo.20015.

1. Introduction

[2] Accompanying the middle Miocene growth of the East Antarctic Ice Sheet (EAIS) are major perturbations in the global carbon system, represented by some of the largest

fluctuations in marine carbonate $\delta^{13}\text{C}$ values in the Cenozoic [Flower and Kennett, 1995; Zachos *et al.*, 2001]. A broad positive carbon isotope excursion (the “Monterey Excursion” [Vincent and Berger, 1985]) begins in the early Miocene (approximately 16.9 Myr ago) and terminates in the middle Miocene (~ 13.6 Myr ago [Holbourn *et al.*, 2007]). Within this broad $\delta^{13}\text{C}$ excursion, higher frequency fluctuations have been recognised with at least seven carbon isotope maxima (CM) defined [Woodruff and Savin, 1991]. These positive carbon isotope excursions are traditionally interpreted as the result of increased burial of organic carbon leading to a drawdown of carbon dioxide from the atmosphere, and subsequent global cooling and ice build-up [Flower and Kennett, 1993a; Vincent and Berger, 1985]. The largest of the carbon isotope maxima (“CM6” [Woodruff and Savin, 1991]) immediately follows the major ice expansion event of the middle Miocene (“E3”; [Flower and Kennett, 1993b] or “Mi-3”; [Miller *et al.*, 1991]) and therefore may represent an important positive feedback in the climate system.

[3] However, it has recently been suggested that carbonate carbon isotope maxima associated with glacial transitions may be evidence of a negative feedback in the climate system [Shevenell *et al.*, 2008]. Under this alternative scenario, ice sheet expansion blankets an area of silicate basement that was previously a sink for atmospheric $p\text{CO}_2$ via silicate weathering [Pagani *et al.*, 1999; Lear *et al.*, 2004; Shevenell *et al.*, 2008; Tian *et al.*, 2009]. Both scenarios could result in

¹School of Earth and Ocean Sciences, Cardiff University, Main Building, Park Place, Cardiff, UK.

²Organic Geochemistry Unit, The Cabot Institute and Bristol Biogeochemistry Research Centre, School of Chemistry, University of Bristol, Bristol, UK.

³School of Earth Sciences, University of Bristol, Wills Memorial Building, Bristol, UK.

⁴Bristol Isotope Group, School of Earth Sciences, University of Bristol, Wills Memorial Building, Bristol, UK.

⁵Now at Ocean and Earth Science, National Oceanography Centre Southampton, University of Southampton Waterfront Campus, Southampton, UK.

⁶Geology Department, Amgueddfa Cymru-National Museum Wales, Cardiff, UK.

⁷Department of Geology, University of Leicester, Leicester, UK and NERC Isotope Geosciences Laboratory, British Geological Survey, Nottingham, UK.

⁸Stratigraphy / Paleontology, Department of Earth Sciences, Utrecht University, Utrecht, The Netherlands.

Corresponding author: Marcus P.S. Badger, School of Earth Sciences, Bristol University, Wills Memorial Building, Queens Rd, Bristol, BS8 1RJ, UK. (marcus.badger@bristol.ac.uk)

positive carbonate carbon isotope excursions: the former by removal of ¹³C-depleted carbon from the ocean-atmosphere reservoir as more organic matter is buried, and the latter by lowering buried organic matter $\delta^{13}\text{C}$ values as a result of increased photosynthetic isotopic fractionation (ϵ_p) due to higher concentrations of dissolved carbon dioxide ($[\text{CO}_{2(\text{aq})}]$). Critically, these scenarios involve opposite changes in atmospheric carbon dioxide concentration. Therefore, to assess the likelihood of these mechanisms, we reconstruct atmospheric $p\text{CO}_2$ following the middle Miocene ice sheet expansion using two independent proxies: alkenone and boron isotope paleobarometry.

2. Materials and Methods

[4] The Blue Clay Formation of Malta (at Ras il-Pellegrin (RIP); Figure 1; 35°54.93'N 14°20.06'E) is a continuous land-based section of Miocene pelagic clays and marls with high sedimentation rates (40 mMyr⁻¹) [Abels *et al.*, 2005] and estimated paleowater depth of 500 to 600 m [Bellanca *et al.*,

2002; Bonaduce and Barra, 2002]. The high clay content of the Blue Clay Formation has resulted in excellent preservation of microfossils, and the simple tectonic history of Malta [Dart *et al.*, 1993] has resulted in material that has never been exposed to high temperatures or pressures, suggesting that primary geochemical signals should be preserved. The transition to the Blue Clay Formation from the older Globigerina Limestone Formation below coincides with the ice volume build-up “E3” [Abels *et al.*, 2005; Woodruff and Savin, 1991]. The associated change in preservation style precludes a continuous record across the entire climate transition. Nevertheless, we sampled the Blue Clay Formation at 35 cm (~9 kyrs) resolution enabling us to generate a stratigraphy of the 1.1 million years following ice volume build-up “E3”. In the field, samples were tied to the lithostratigraphic log of Abels *et al.* [2005]. Subsequent refinement was achieved by matching bulk isotope stratigraphies. The astronomical recalibration of the lower part of the Blue Clay Formation according to Mourik *et al.* [2011] was used for the age model.

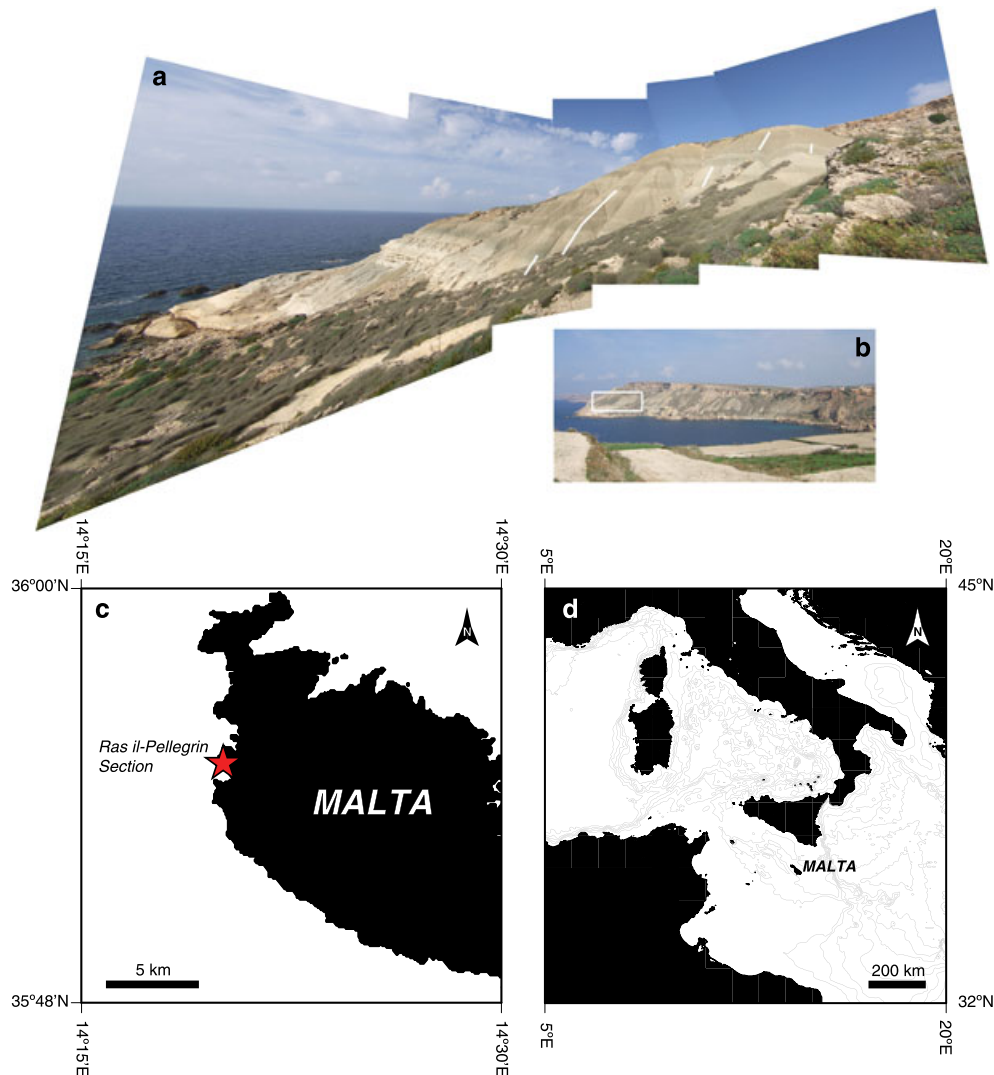


Figure 1. The Ras il-Pellegrin section (35°54.93'N 14°20.06'E). (a) Sampling site, with positions of sampling trenches shown in white (b) View towards the sampling site (marked by white rectangle) across Fomm Ir-Rih Bay (c) Location of sampling site (red star) on the island of Malta (d) Location of Malta in the central Mediterranean Sea.

[5] We analysed bulk and fine fraction (<63 μm) carbonate for $\delta^{13}\text{C}$ and $\delta^{18}\text{O}$, and the planktic foraminifera *Globigerinoides trilobus* for Mg/Ca, $\delta^{13}\text{C}$, $\delta^{18}\text{O}$, B/Ca, and $\delta^{11}\text{B}$. We also generated a compound specific (C_{37} alkenone) carbon isotope record.

2.1. Carbonate Stable Isotope Stratigraphy

[6] Bulk sediment and foraminiferal isotope analyses were performed on a ThermoFinnigan MAT 252 with online sample preparation using an automated Kiel III carbonate device at Cardiff University. Long term uncertainties based on repeat analysis of NBS-19 are $\pm 0.08\text{‰}$ and $\pm 0.05\text{‰}$ for $\delta^{18}\text{O}$ and $\delta^{13}\text{C}$ respectively (2σ). Fine fraction isotope samples (<63 μm) were prepared offline and resultant CO₂ analysed using a VG Optima dual inlet gas source mass spectrometer at the NERC Isotope Geosciences Laboratory, analytical uncertainties are typically $\pm 0.2\text{‰}$ for both $\delta^{18}\text{O}$ and $\delta^{13}\text{C}$ (2σ). All isotope data are reported as per mil on the VPDB scale.

2.2. Planktic Foraminiferal Mg/Ca Analyses

[7] Between 19 and 30 individuals of *G. trilobus* were picked from the 250–355 μm size fraction and cleaned following the procedure of *Barker et al.* [2003]. In the modern ocean, *G. trilobus* is considered to be the same biological species as *G. sacculifer*, although *G. sacculifer* apparently did not evolve until the Pliocene [*Hemleben et al.*, 1989]. Here we assume *G. trilobus* and *G. sacculifer* are the same species. Samples were dissolved in 0.065 M nitric acid and analysed by sector field inductively coupled plasma mass spectrometry Thermo Scientific ELEMENT-XR (ICP-MS) at Cardiff University. Each sample was calibrated against a standard with matched Ca concentration to reduce matrix effects. Long-term analytical precision is better than 2 % (r.s.d.).

2.3. Organic Geochemistry

[8] 5 g powdered samples were saponified and ultrasonically extracted using sequentially, methanolic 0.1 M KOH (5 % H₂O), methanol and a 3:1 (v/v) azeotrope of dichloromethane (DCM):methanol. Neutral fractions were obtained from the total extract by liquid-liquid separation with *n*-hexane:DCM (9:1 v/v) and silica gel column chromatography was used to divide samples into four fractions (F), eluted sequentially with *n*-hexane (4 ml, Fraction 1), *n*-hexane:DCM (2:1 v/v; 2 ml, F2), DCM (5 ml, F3) and DCM:Methanol (95:5 v/v; 5 ml, F4). Alkenones elute in F3, and their quantification for $U_{37}^{K'}$ calculation was performed on a Carlo Erba Instruments HRGC5300 gas chromatogram (GC) fitted with a flame ionisation detector and a Chrompack fused silica capillary column (50 m \times 0.32 mm internal diameter; CP Sil-5CB stationary phase, dimethylpolysiloxane equivalent, 0.12 μm film thickness). Compound specific carbon isotope analyses were performed on a Finnigan MAT Delta S coupled to a GC with on-column injector using a modified Finnigan MAT Type 1 GC combustion interface at the University of Bristol. A Zebron ZB-1 fused silica capillary column (50 m \times 0.32 mm internal diameter; dimethylpolysiloxane equivalent stationary phase, 0.12 μm film thickness) was used. Samples were injected at 70°C, and the oven programmed to increase in temperature to 130°C at 20 °Cmin⁻¹ then to 300°C at 4°Cmin⁻¹, remaining isothermal

at 300°C for 25 minutes. Long term uncertainties, on the basis of repeat standard measurements, are $\pm 0.6\text{‰}$ (2σ).

2.4. Foraminiferal $\delta^{11}\text{B}$ and B/Ca Analyses

[9] Six samples of *G. trilobus* (250–355 μm) each consisting of around 100 tests ($\sim 2\text{ mg}$ of CaCO₃) were analysed for their boron isotopic composition on a ThermoFinnigan NEPTUNE multicollector ICP-MS at the University of Bristol following the methodology described by *Foster* [2008]. Analytical precision of this approach is $\pm 0.23\text{‰}$ at 95 % confidence as determined by the long term reproducibility of full procedural replicates of an in-house coral standard. Prior to isotope analysis, but following cleaning and dissolution, an aliquot of each sample was analysed for trace element content using a sector field ThermoFinnigan ELEMENT 2 ICP-MS [*Foster*, 2008; *Ni et al.*, 2007] at the University of Bristol. This analysis ensured cleaning was successful and provided a measure of the B/Ca ratio for each sample. The long-term reproducibility of our in house consistency standards for B/Ca is $\pm 2\%$ (95% confidence) and our accuracy is better than 5% [*Ni et al.*, 2007].

2.5. Mg/Ca Paleotemperature Equation

[10] Critical to the accuracy of the alkenone and, to a lesser extent, the boron $p\text{CO}_2$ reconstruction is an accurate record of sea surface temperature (SST). However, foraminiferal calcite Mg/Ca is controlled not only by temperature, but also the Mg/Ca ratio of the seawater in which they calcify. The application of this proxy beyond the oceanic residence time of Ca and Mg (1 and 22 Myrs respectively; *Fantle and DePaolo* [2005, 2006]) can therefore be complicated by changes in seawater Mg/Ca ratios ($\text{Mg}/\text{Ca}_{\text{sw}}$) with time. This is often corrected for by assuming a linear relationship between seawater Mg/Ca and foraminiferal Mg/Ca [e.g., *Lear et al.*, 2000] although it has been suggested that this dependency may be better described using a power function [*Hasiuk and Lohmann*, 2010] (equation 1).

$$(\text{Mg}/\text{Ca})_{\text{foram}} = (\text{Mg}/\text{Ca}_{\text{sw}(t)} / \text{Mg}/\text{Ca}_{\text{sw}(0)})^C \cdot \text{Be}^{AT} \quad (1)$$

Where $\text{Mg}/\text{Ca}_{\text{foram}}$ is the Mg/Ca ratio of foraminiferal calcite, $\text{Mg}/\text{Ca}_{\text{sw}(0)}$ and $\text{Mg}/\text{Ca}_{\text{sw}(t)}$ are the Mg/Ca ratios of seawater today and at time t respectively, A , B , and C are constants ('exponential', 'pre-exponential' and 'power' respectively) and T is temperature.

[11] Mg and Ca are both delivered to the oceans via rivers and removed into sediments including carbonates. Hydrothermal alteration of basalt at ocean ridge systems represents an important sink for magnesium and source for calcium. All of these fluxes have varied over time. The residence times of Ca and Mg mean that $\text{Mg}/\text{Ca}_{\text{sw}}$ is unlikely to have varied significantly over the duration of our record, but may have been considerably different in the Miocene compared to the present day. Attempts have been made to reconstruct $\text{Mg}/\text{Ca}_{\text{sw}}$ over time using geochemical models [*Hardie*, 1996; *Wilkinson and Algeo*, 1989, *Fantle and DePaolo*, 2005; 2006], echinoderm skeletons [*Dickson*, 2002, 2004], fluid inclusions in marine evaporites [*Lowenstein et al.*, 2001, *Horita et al.*, 2002] and carbonate veins precipitated in oceanic basalt [*Coggon et al.*, 2010]. Although these various reconstructions agree that $\text{Mg}/\text{Ca}_{\text{sw}}$ was lower during the Miocene than today, its precise value remains unclear.

[12] Here we apply the fluid inclusion based Mg/Ca_{sw} value of *Horita et al.* [2002] (Mg/Ca_{sw} = 3.43) to the generic planktic Mg/Ca paleotemperature equation of *Anand et al.* [2003] (A = 0.09, B = 0.38 in equation 1), and apply the power constant for *G. sacculifer* (C = 0.41 in equation 1) as determined by *Evans and Müller* [2012] based on the data of *Delaney et al.* [1985]. This results in the Mg/Ca_{sw} corrected paleotemperature equation given in equation 2.

$$Mg/Ca_{foram} = 0.32e^{0.09T} \quad (2)$$

[13] The fluid inclusion data has the advantage over other methods of also providing absolute values for [Mg] and [Ca], as required to reconstruct carbonic acid dissociation constants K₁ and K₂ (see section 2.7).

2.6. Alkenone Paleobarometry

[14] Isotopic fractionation between dissolved inorganic carbon (DIC) and algal biomass (ϵ_p) occurs during photosynthesis and is strongly controlled by [CO_{2(aq)}] [*Laws et al.*, 1995], a relationship that serves as the basis of the phytoplankton-based pCO₂ paleobarometer [*Hollander and McKenzie*, 1991; *Pagani et al.*, 1999]. However, a range of other factors, including algal growth rate and cell geometry also govern ϵ_p values [*Bidigare et al.*, 1997; *Popp et al.*, 1998a]. In order to control source organism and restrict cell size effects, we measure the carbon isotopic composition of C₃₇ alkenones ($\delta^{13}C_{37}$). C₃₇ alkenones are long chain methyl ketones produced by a restricted group of haptophyte algae [*Marlowe et al.*, 1990] and have been used in several studies to reconstruct levels of atmospheric carbon dioxide over time [*Jasper et al.*, 1994; *Pagani et al.*, 2005; *Seki et al.*, 2010]. Haptophyte biomass $\delta^{13}C$ values can be determined by correcting $\delta^{13}C_{37}$ for the biosynthetic offset of 4‰ [*Popp et al.*, 1998a]; ϵ_p values are then determined by reconstructing the carbon isotopic composition of dissolved CO₂ ($\delta^{13}C_{[CO_2(aq)]}$). Shallow dwelling foraminifera have been used previously to determine the DIC $\delta^{13}C$ value used for alkenone paleobarometry. However, the low number of individuals available for analysis here results in a record with a low signal to noise ratio. We therefore estimate surface water DIC $\delta^{13}C$ using fine fraction $\delta^{13}C_{carb}$, with an isotopic offset of +2‰ calculated from the mean difference between *G. trilobus* $\delta^{13}C$ and $\delta^{13}C_{carb}$ over CM6. Using this $\delta^{13}C$ record we determine $\delta^{13}C_{[CO_2(aq)]}$ with temperature dependant fractionation quantified using Mg/Ca paleothermometry as described above. Calculated ϵ_p values were converted to [CO_{2(aq)}] using the relationship determined by *Bidigare et al.* [1997] assuming a growth rate (phosphate) dependant b-value of 110.65 for *Emiliania huxleyi*, which is typical for oligotrophic regimes [e.g. *Bidigare et al.*, 1997; *Pagani et al.*, 2010]. Atmospheric pCO₂ is then calculated by applying Henry's law, assuming equilibrium between ocean-atmosphere CO₂ and again using reconstructed SSTs; where necessary, SST was estimated on the basis of linear interpolation in the time domain.

[15] Uncertainty propagation on our alkenone-derived pCO₂ estimates was performed by Monte Carlo modeling (n = 25000). Salinity uncertainty was estimated by reconstructing $\delta^{18}O_{sw}$ using paired *G. trilobus* Mg/Ca SST and $\delta^{18}O$ data, assuming all variation in $\delta^{18}O_{sw}$ was due to

salinity variations using the sensitivity described in *Maslin et al.* [1995]. This approach produces a maximum uncertainty as most of the variability in $\delta^{18}O_{sw}$ will be due to changing ice volume. Uncertainties of 2°C and 0.2‰ were applied to temperature and $\delta^{13}C_{carb}$, respectively (normal probability density function (pdf), 2σ error) and 2.5 mmol and 0.05 psu on salinity and [PO₄³⁻] respectively (uniform pdf). 2σ errors on $\delta^{13}C_{37}$ were estimated from replicate runs. An 11% error on the slope of b = a[PO₄] + c was assumed [*Pagani et al.*, 1999].

2.7. Boron Based Paleobarometry

[16] There are two isotopes of boron, ¹⁰B and ¹¹B, with natural abundances of ~20 % and ~80 %, respectively. Isotope variations are described in delta notation as follows:

$$\delta^{11}B = \left[\left(\frac{{}^{11}B/{}^{10}B_{sample}}{{}^{11}B/{}^{10}B_{NIST951}} \right) - 1 \right] \times 1000 \quad (3)$$

where ¹¹B/¹⁰B_{NIST951} is the ¹¹B/¹⁰B ratio of NIST SRM 951 boric acid standard (¹¹B/¹⁰B = 4.04367; *Catanzaro et al.* [1970]).

[17] Boron exists as two species in aqueous solutions at typical ocean pH: boric acid (B(OH)₃) and borate ion (B(OH)₄⁻). The abundance of these species is pH dependent with ~80 % B(OH)₃ at typical seawater pH. Due to structural differences between the two boron species in seawater there is a pronounced isotopic fractionation between them in seawater, with B(OH)₃ being enriched in ¹¹B. In order to maintain a constant $\delta^{11}B$ of seawater, the isotopic composition of each species also varies according to pH, for instance, the isotopic composition of B(OH)₄⁻ is related to pH by the following:

$$pH = pK_B^* - \log \left(\frac{\delta^{11}B_{B_{sw}} - \delta^{11}B_{B(OH)_4^-}}{\delta^{11}B_{B_{sw}} - \alpha_B \cdot \delta^{11}B_{B(OH)_4^-} - ((\alpha_B - 1) \cdot 1000)} \right) \quad (4)$$

where pK_B^{*} is the -log₁₀ of the stoichiometric equilibrium constant for boric acid [*Dickson*, 1990] at the *in situ* temperature, salinity and pressure, $\delta^{11}B_{sw}$ is the isotopic composition of seawater (39.61‰; *Foster et al.* [2010]), $\delta^{11}B_{B(OH)_4^-}$ is the isotopic composition of borate ion. The isotopic fractionation between the two aqueous species of boron in seawater (α_B) has recently been determined as 1.0272 ± 0.0006‰ [*Klochko et al.*, 2006].

[18] On the basis of isotopic measurements of marine carbonates, *Hemming and Hanson* [1992] suggested that the borate ion species is preferentially incorporated into marine carbonate. However, NMR studies [*Klochko et al.*, 2009] have shown that some trigonal BO₃ is also present in CaCO₃ which has been used by some to argue that boric acid may also be incorporated into CaCO₃. Recent isotopic measurements of benthic foraminifera by MC-ICP-MS however confirm that only very minor amounts of boric acid can be incorporated in foraminifera (<1 %; *Rae et al.* [2011]). Consequently, for epifunal benthic foraminifera measured by MC-ICP-MS $\delta^{11}B_{foram} = \delta^{11}B_{B(OH)_4^-}$, and equation (4) can be used to calculate pH.

[19] For the planktic foraminifera *G. trilobus* used here (assuming *G. trilobus* is the same as *G. sacculifer*), it has been shown [*Sanyal et al.*, 2001], using negative ion thermal ionisation mass spectrometry (NTIMS), that there was a

strong pH dependency of $\delta^{11}\text{B}$ but $\delta^{11}\text{B}_{\text{foram}} \neq \delta^{11}\text{B}_{\text{B(OH)}_4^-}$. Here we follow *Foster et al.* [2012] in order to correct for these “vital effects” and calculate $\delta^{11}\text{B}_{\text{B(OH)}_4^-}$ from the $\delta^{11}\text{B}$ of *G. trilobus* (300-355 μm) by:

$$\delta^{11}\text{B}_{\text{B(OH)}_4^-} = \delta^{11}\text{B}_{\text{trilobus}} \times 0.88 + 1.85 \quad (5)$$

[20] The $\delta^{11}\text{B}_{\text{B(OH)}_4^-}$ can then be inserted into equation (4) to calculate pH. Since *G. trilobus* is a predominantly mixed layer dweller, we assume that the calculated pH is that of surface water.

[21] The stoichiometric dissociation constant of boric acid (K^*_B) is temperature, salinity and pressure dependent [Dickson, 1990]. These variables do not have a large impact on the calculated pH and $p\text{CO}_2$ (e.g. ~ 10 ppm/ $^\circ\text{C}$; ~ 2 ppm/psu) and here salinity is assumed to be 35 psu throughout and SST is given by *G. trilobus* Mg/Ca as detailed above.

[22] From equation (4) it can be seen that use of $\delta^{11}\text{B}$ in *G. trilobus* to reconstruct pH and hence $p\text{CO}_2$ requires an estimate of the isotopic composition of seawater in the past. The oceanic residence time of boron is ~ 14 Myrs [Lemarchand et al., 2002], and modeling approaches suggest that the seawater boron isotope ratio was lower by up to a few per mil during the Miocene, but the absolute magnitude of the change in seawater $\delta^{11}\text{B}$ is largely uncertain [Lemarchand et al., 2002; Simon et al., 2006; Pearson and Palmer, 2000; Paris et al., 2010]. Using a modification of the depth profile approach of Pearson and Palmer [2000], Foster et al. [2012] calculate $\delta^{11}\text{B}_{\text{sw}}$ was 37.8‰ for the middle Miocene, a value that is in good agreement with the modeling of Lemarchand et al. [2002] and the reconstruction of Pearson and Palmer [2000]. Given the long residence time of boron in seawater (~ 14 Myrs; [Lemarchand et al., 2002]), that value is likely appropriate for our entire record.

[23] To fully reconstruct changes in the ocean carbonate system, two of the six co-varying parameters (pH, $[\text{CO}_{2(\text{aq})}]$, $[\text{HCO}_3^-]$, $[\text{CO}_3^{2-}]$, Total Alkalinity and DIC) must be known. Foster et al. [2012] calculate surface water alkalinity for the middle Miocene using a modeling approach that closely follows Tyrrell and Zeebe [2004] supplemented with new $\delta^{11}\text{B}$ measurements of benthic foraminifera to estimate deep water pH. By assuming a similar to modern surface to deep alkalinity gradient, Foster et al. [2012] estimate surface water total alkalinity in the middle Miocene to be 1293 ± 200 $\mu\text{mol/kg}$. The uncertainty in this estimate accounts for uncertainties in the surface-deep gradient, the depth of carbonate compensation depth, and any variations in total alkalinity during the course of our record (see Foster et al. [2012] for details). The uncertainties in $p\text{CO}_2$ we calculate from the boron based-pH are dominated by uncertainties in this second carbonate system parameter (± 40 ppm). A quadratic addition of other likely uncertainties, e.g., temperature (± 1 $^\circ\text{C}$) and $\delta^{11}\text{B}$ (around ± 20 ppm), gives a total uncertainty of approximately ± 50 ppm. It is important to note that following Tyrrell and Zeebe [2004] we also account in all carbonate system calculations for the effect of changing [Mg] and [Ca] of seawater on the carbonic acid dissociation constants K_1 and K_2 and the solubility product of CaCO_3 (K_{sp}), by using the [Ca], [Mg], and Mg/Ca_{sw} taken from the fluid inclusion data of Horita et al. [2002].

[24] The pH dependent speciation of boron in seawater also forms the basis for the B/Ca proxy of the carbonate

system. It is thought that the incorporation of boron into calcium carbonate can be described by the following equilibria [Hemming and Hanson, 1992]:



[25] Following Zeebe and Wolf-Gladrow [2001] the following exchange equilibria (K_D) can be defined:

$$K_D = \left(\frac{B/\text{Ca}_{\text{solid}}}{B(\text{OH})_4^-/\text{HCO}_3^- \text{ seawater}} \right) \quad (7)$$

[26] It therefore follows that, since the B(OH)_4^- concentration is pH dependent, if K_D can be calibrated and the pH determined (e.g. using boron isotopes), equation (4) can be solved for HCO_3^- providing a second variable of the carbonate system which would allow the whole system to be resolved. However, the K_D for planktic species such as *G. sacculifer* has been shown to be species specific and dependent on test size [Ni et al., 2007] as well as one or several environmental variables (e.g. temperature and/or $[\text{CO}_3^{2-}]$; [Yu et al., 2007; Foster, 2008]). A recent culture study has shown that for *G. sacculifer*, temperature had a negligible effect on boron incorporation but K_D was inversely proportional to $[\text{CO}_3^{2-}]$, perhaps as a consequence of $[\text{CO}_3^{2-}]$ competing with B(OH)_4^- for the same lattice site [Foster et al., 2008; Allen et al., 2011, 2012; Allen and Hönisch, 2012]. Although Foster [2008] presents a core top calibration for *G. sacculifer* (500-600 μm) the relationships between K_D and temperature and $[\text{CO}_3^{2-}]$ remain rather poorly defined [Allen and Hönisch, 2012]. Furthermore, as the evolution of seawater [B] over these timescales is also unknown, we consider that a more quantitative treatment of our B/Ca data would be somewhat premature.

2.8. Carbon Cycle Modeling

[27] We use the mass balance model of Kump and Arthur [1999] to calculate changes in the isotopic composition of inorganic and organic carbon in the ocean/atmosphere system. Changes in the modeled carbon content of the system are driven by changing inputs from weathering and metamorphism/volcanism and outputs from the burial of carbon as carbonate minerals and organic matter. The model accounts for changing ϵ_p values due to varying $p\text{CO}_2$ and we also include a negative weathering feedback on changing $p\text{CO}_2$ as detailed by Kump and Arthur [1999]:

$$F_{\text{wsil}}^{\text{t}} = F_{\text{wsil}}^0 \cdot \left[p\text{CO}_2^{\text{(t)}} / p\text{CO}_2^{\text{(0)}} \right] \quad (8)$$

where F_{wsil} is the global silicate weathering flux. In order to simulate Miocene climate we set initial $p\text{CO}_2$ at 330 ppm (derived from our alkenone paleobarometry results) and ran the models for 1 Myrs to reach steady state before starting perturbations. Models were solved numerically using MATLAB (Simulink) with variable step solver ode45.

3. Results and Discussion

[28] Our bulk carbonate oxygen isotope record ($\delta^{18}\text{O}_{\text{carb}}$) shows the final step (“E3”) of the globally recognised increase in $\delta^{18}\text{O}$ at the MMCT, and our fine fraction (< 63 μm) carbonate carbon isotope record ($\delta^{13}\text{C}_{\text{carb}}$) shows the

distinctive double peak of CM6, confirming that the RIP section faithfully records global changes (Figure 2). Alkenone $\delta^{13}\text{C}$ ($\delta^{13}\text{C}_{37}$) values are somewhat variable, but display an overall increase across CM6 (Figure 3). The boron-based proxy data are limited to the older portion of CM6 due to sample availability, but nevertheless also display a consistent increase (Figure 3).

[29] *G. trilobus* Mg/Ca ratios decrease from 6.6 mmol/mol at the start of the record at 13.799 Ma, to 3.9 mmol/mol by 13.021 Ma (Table 1). For much of the early part of the record only the di-unsaturated alkenone is present suggesting SSTs exceeded 29°C (Table 1; [Müller *et al.*, 1998]); this could reflect enhanced degradation of the tri-unsaturated alkenone, but such differential degradation, even under highly oxidising conditions, appears to increase $U_{37}^{K'}$ by only ~0.1 (equivalent to <0.5°C; [Huguet *et al.*, 2009]). Moreover, the tri-unsaturated alkenone is present in younger sediments, and $U_{37}^{K'}$ indices reach a minimum value of 0.91 at 13.709 Ma. The high Mg/Ca ratios and $U_{37}^{K'}$ indices suggest high SSTs (> 29°C) at this point in the Miocene; the SST record determined using our Mg/Ca calibration (equation (2)) indicates a decrease of about 4°C following the ice sheet expansion, independent of the value of Mg/Ca_{sw} (Figure 4). We note that even given the large uncertainties surrounding Mg/Ca_{sw} and the response of foraminifera to changing Mg/Ca_{sw}, our Mg/Ca SST estimates are predominantly within uncertainty of our $U_{37}^{K'}$ based estimates (Figures 4 and 5), providing support for the power law approach of Evans and Müller [2012].

[30] Our calculated ε_p values are almost identical to published Miocene values [Pagani *et al.*, 1999] determined from similar aged oligotrophic regions, giving us confidence that growth rate effects were minimal in the RIP section, and that the reconstructed $p\text{CO}_2$ is a global, rather than local signature [Pagani *et al.*, 1999] (Figure 5). Our calculated $p\text{CO}_2$ levels of 260 to 350 ppm are slightly higher than those reported previously (~240 ppm) [Pagani *et al.*, 1999, 2005]. This difference is due to our higher SST estimates, which affect air-sea CO₂ equilibria. Post-depositional preservation effects at the deep-sea carbonate-rich sites used by Pagani *et al.* [1999] almost certainly resulted in artificially cool temperature estimates from oxygen isotope paleothermometry [Pearson *et al.*, 2001], and recently revised Miocene $p\text{CO}_2$ estimates are similar to those observed here [Pagani *et al.*, 2010]. The clay-rich lithology at RIP has resulted in excellent preservation of foraminifera enabling more accurate estimates of past SST using Mg/Ca paleothermometry. These differences result in alkenone $p\text{CO}_2$ estimates that are somewhat higher than previously reported by Pagani *et al.* [1999, 2005] but are still generally low (~300 ppm) and comparable to those measured in other Neogene studies [Kürschner *et al.*, 2008; Foster *et al.*, 2012] (Figure 5).

[31] *G. trilobus* $\delta^{11}\text{B}$ values increase across CM6 (Figure 3), which implies an increasing pH and decreasing $p\text{CO}_2$ regardless of our choice of seawater $\delta^{11}\text{B}$ (Table 2) or second carbonate system parameter. In support of this conclusion, we note that our *G. trilobus* B/Ca record also increases across CM6 (Figure 3), which, in the absence of

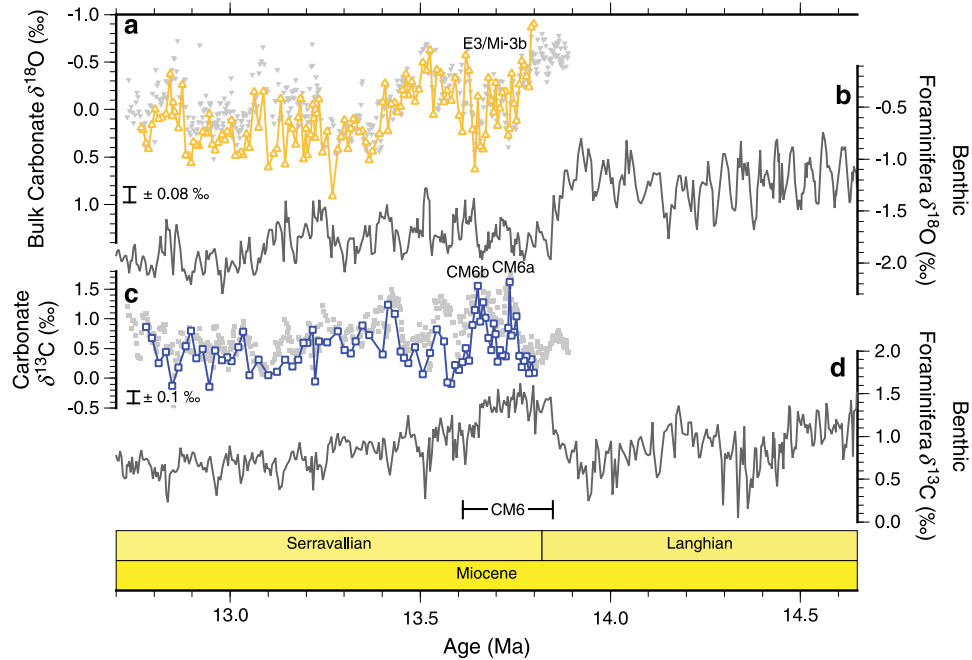


Figure 2. Multi-proxy records following the middle Miocene Antarctic ice sheet expansion. (a) Bulk carbonate oxygen isotope record from the Ras il-Pellegrin section (this study, orange open triangles and line, Abels *et al.* [2005], gray inverted triangles) (b) Benthic foraminiferal $\delta^{18}\text{O}$ record from ODP Site 1146 (gray line; [Holbourn *et al.*, 2005]) (c) Carbonate carbon isotope records from the Ras il-Pellegrin section (fine fraction $\delta^{13}\text{C}$ from this study, blue open squares and line, and bulk carbonate $\delta^{13}\text{C}$ from Abels *et al.* [2005], gray filled squares) (d) Benthic foraminiferal $\delta^{13}\text{C}$ record from ODP Site 1146 (gray line; [Holbourn *et al.*, 2005]). Age models for all records have been retuned following Mourik *et al.* [2011]. Error bars shown are $\pm 2\sigma$.

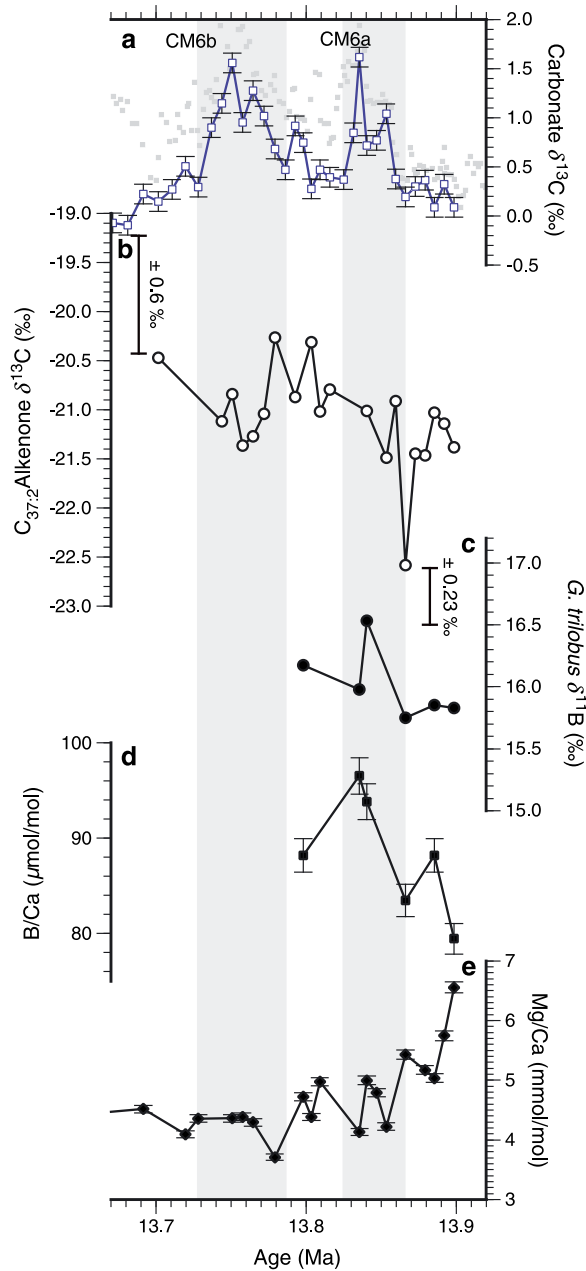


Figure 3. Isotope and trace metal records across CM6 from the Ras il-Pellegrin section. (a) Carbonate $\delta^{13}\text{C}$ from fine fraction (this study; blue open squares and line) and bulk carbonate (Abels *et al.* [2005]; gray filled squares) (b) alkenone $\delta^{13}\text{C}$ (open circles and line) (c) *G. trilobus* $\delta^{11}\text{B}$ (filled circles and line) (d) *G. trilobus* B/Ca ratios (black filled squares) and (e) *G. trilobus* Mg/Ca ratios. Error bars shown are $\pm 2\sigma$.

other complicating factors [Yu *et al.*, 2007; Foster, 2008; Allen *et al.*, 2011], also implies an increase in surface water pH and hence decrease in $p\text{CO}_2$ [Foster, 2008].

[32] Using a $\delta^{11}\text{B}_{\text{sw}} = 37.8\text{‰}$ [Foster *et al.*, 2012], $\delta^{11}\text{B}$ -based pH changes from 7.91 ± 0.03 to a maximum of 8.02 ± 0.03 . Using this pH record, along with a total alkalinity of $1293 \pm 200 \mu\text{mol}$, yields $p\text{CO}_2$ estimates that drop from $311 \pm 55 \text{ ppm}$ to a minimum of $230 \pm 43 \text{ ppm}$ ($\Delta p\text{CO}_2$

Table 1. U_{37}^K Temperatures and Planktic Foraminiferal (*G. trilobus*) Mg/Ca and Mg/Ca-Temperatures From the Blue Clay Formation at Ras il-Pellegrin, Malta

Height in Section (m)	Age [Mourik <i>et al.</i> , 2011] (Ma)	U_{37}^K	SST ^a [Müller <i>et al.</i> , 1998] (°C)	<i>G. trilobus</i> Mg/Ca Ratio (mmol/mol)	SST (°C)
0.00	13.799	1	29.0*	6.56	33.5
0.35	13.792	1	29.0*	5.74	32.0
0.70	13.786	1	29.0*	5.03	30.6
1.05	13.779	1	29.0*	5.17	30.9
1.75	13.766	1	29.0*	5.43	31.4
2.45	13.753	1	29.0*	4.22	28.6
2.80	13.747			4.79	30.0
3.15	13.741	1	29.0*	5.00	30.5
3.50	13.736	1	29.0*	4.13	28.4
3.85	13.731	1	29.0*	4.78	30.0
4.90	13.709	0.909	26.2	4.97	30.4
5.25	13.704	0.985	28.5	4.38	29.0
5.60	13.698	0.987	28.6	4.72	29.9
6.65	13.679	1	29.0*	3.71	27.2
7.35	13.665	0.981	28.4	4.29	28.8
7.70	13.658	1	29.0*	4.39	29.0
8.05	13.651	1	29.0*	4.36	29.0
8.40	13.644	1	29.0*		
9.10	13.628	0.997	28.9	4.36	29.0
9.45	13.620	1	29.0*	4.09	28.3
10.15	13.602	0.979	28.3		
10.50	13.592			4.52	29.4
11.20	13.571	0.960	27.8		
18.20	13.408	0.967	28.0		
22.75	13.301	0.964	27.9	3.92	27.8
33.95	13.021	0.978	28.3	3.86	27.6
43.05	12.811	0.987	28.6		

^aNote that the U_{37}^K paleothermometer cannot be used for temperatures greater than 29°C, so temperatures marked with a * should be considered minimum estimates.

of ~80 ppm). Importantly, these new $p\text{CO}_2$ estimates using boron isotopes are in very good agreement with our alkenone-based estimates (Figure 4), which provide confidence in the validity of the $\delta^{11}\text{B}_{\text{sw}}$ and total alkalinity reconstructions of Foster *et al.* [2012]. Boron isotope compositions of *G. trilobus* from the RIP section are also very similar to middle Miocene aged *G. trilobus* measured by MC-ICP-MS by Foster *et al.* [2012] from ODP Site 761 and Site 926.

4. The Miocene Carbon Cycle and Climate

[33] Our $\delta^{13}\text{C}_{37}$, B/Ca and $\delta^{11}\text{B}$ records show positive trends over CM6 (Figure 3); for the former, this yields a decrease in ε_p values. Therefore, regardless of the absolute values or treatment of Mg/Ca_{sw} , the alkenone and boron based- CO_2 proxies all indicate CM6 is associated with a $p\text{CO}_2$ decrease (Figure 4). In order to evaluate potential causes of CM6, we ran a simple ocean carbonate system model [Kump and Arthur, 1999] to assess the feasibility of the organic matter burial hypothesis. We inverse model the $\delta^{13}\text{C}_{\text{carb}}$ increase by assuming it is driven by two discrete pulses of increased organic carbon burial. Under this scenario, the magnitude of the $\delta^{13}\text{C}_{\text{carb}}$ increase across CM6a and CM6b requires a 70% and a 50% increase in organic carbon burial respectively, with each perturbation lasting 41 kyrs (inset; Figure 6a). This results in a 60 ppm CO_2 drawdown, which is in agreement with both our alkenone and boron $p\text{CO}_2$ records (Figure 6). This is in contrast to

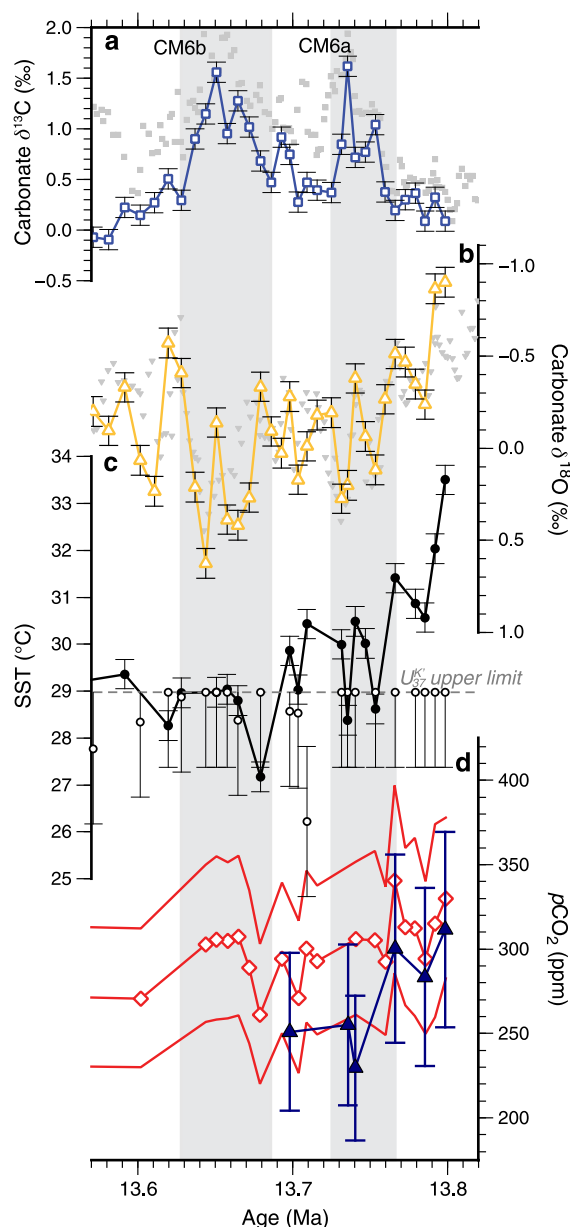


Figure 4. Isotope, temperature and $p\text{CO}_2$ records across CM6 from the Ras il-Pellegrin section (a) Carbonate stable carbon isotopes from fine fraction (this study; blue open squares and line) and bulk carbonate (Abels *et al.* [2005]; gray filled squares), (b) Bulk carbonate oxygen isotopes from this study (orange open triangles and line) and Abels *et al.* [2005] (gray inverted triangles), (c) SST calculated from *G. trilobus* Mg/Ca (filled black circles and line) and from alkenone unsaturation index (open black circles), and (d) atmospheric $p\text{CO}_2$ reconstructions from alkenone isotopes (red open diamonds and solid line with $\pm 2\sigma$ error envelopes) and from boron isotopes (dark blue filled triangles and solid line with propagated analytical uncertainties shown as error bars).

the silicate-weathering hypothesis which would have led to an increase in $p\text{CO}_2$.

[34] The model and the records cannot be used to identify a cause of the suggested increase in organic matter burial (i.e., production versus preservation), which prevents a

useful feasibility assessment of this modeled scenario. Nevertheless, we note that the magnitude of the organic carbon burial increase required to produce the observed carbon isotope excursion is substantial, and suggests that other factors may also have been involved. Although our preferred causal mechanism for CM6 involves at least some component of increased organic carbon burial, we cannot rule out other influences on the size and carbon isotopic composition of the ocean-atmosphere reservoir. For example, cooler bottom water temperatures could have facilitated increased sequestration of methane in hydrates, which would represent a reduced flux of ^{13}C -depleted carbon to the atmosphere from the marine realm. Moreover, our model and records do not distinguish between increased organic matter sequestration in marine vs terrestrial realms or, in the case of the former, between burial at continental margins or in the deep sea. However, export productivity records from the Atlantic do show a pronounced increase over CM6 [Diester-Haass *et al.*, 2009], and there is correlation between the presence of organic-rich sediments and carbon isotope maxima within the Monterey formation [Flower and Kennett, 1993a], suggesting that increased burial of organic matter in the marine realm was likely responsible for a major component of the global $\delta^{13}\text{C}_{\text{carb}}$ excursion.

[35] Our records reveal that organic carbon burial during CM6 could have acted as an important positive feedback on ice sheet growth. Global cooling and sea-level fall associated with the initial growth of the ice sheet would have increased meridional thermal gradients and may have increased ocean ventilation [Flower and Kennett, 1993a]. This may have led to enhanced biological productivity and CO_2 drawdown as a result of a stronger biological pump, and consequently further cooling [Flower and Kennett, 1993a; Vincent and Berger, 1985]. Thus, CM6 likely illustrates an important positive feedback in the global climate system as opposed to a negative feedback [Shevenell *et al.*, 2008] or a primary forcing mechanism [Vincent and Berger, 1985] as has been previously suggested.

5. Summary and Conclusions

[36] The largest of the middle Miocene “carbon maxima” events was associated with a $p\text{CO}_2$ decrease of 59 ± 63 ppm (from $\delta^{13}\text{C}_{37}$) or 82 ± 72 ppm (from $\delta^{11}\text{B}_{\text{trilobus}}$) (e.g. $\sim 20\%$). Both the magnitude and direction of the isotopic shift and observed $p\text{CO}_2$ change are consistent with an increase in organic carbon burial, perhaps fueled by increasing oceanic temperature gradients and overturning following the expansion of the Antarctic ice sheet. At this time, we estimate atmospheric $p\text{CO}_2$ was near 300 ppm, somewhat higher than previous alkenone- [Pagani *et al.*, 1999] and boron-based [Pearson and Palmer, 2000] techniques but in agreement with more recently published long term records [Kürschner *et al.*, 2008; Foster *et al.*, 2012]. We attribute these differences to the use of higher sea surface temperatures in the case of the alkenone estimates and more accurate $\delta^{11}\text{B}$ determinations. Crucially, our estimates suggest an emerging consensus for Miocene $p\text{CO}_2$ between the alkenone, boron isotope and leaf stomatal approaches (Figure 5). Moreover, these values are only slightly higher than modern pre-industrial values and overlap with the threshold values thought to be required for bipolar glaciation [~ 280 ppm; DeConto *et al.*, 2008]. Recent modeling studies suggest that

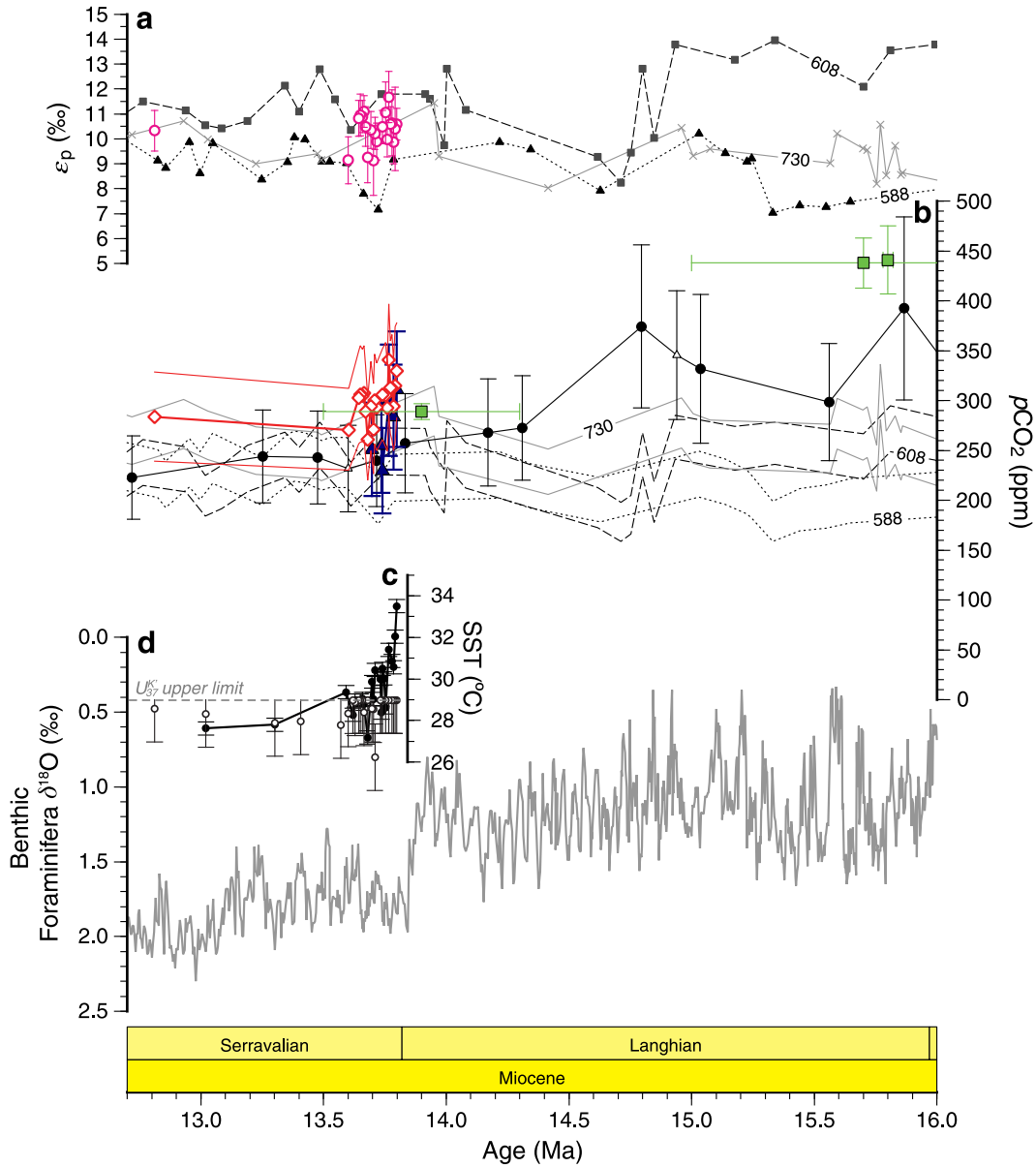


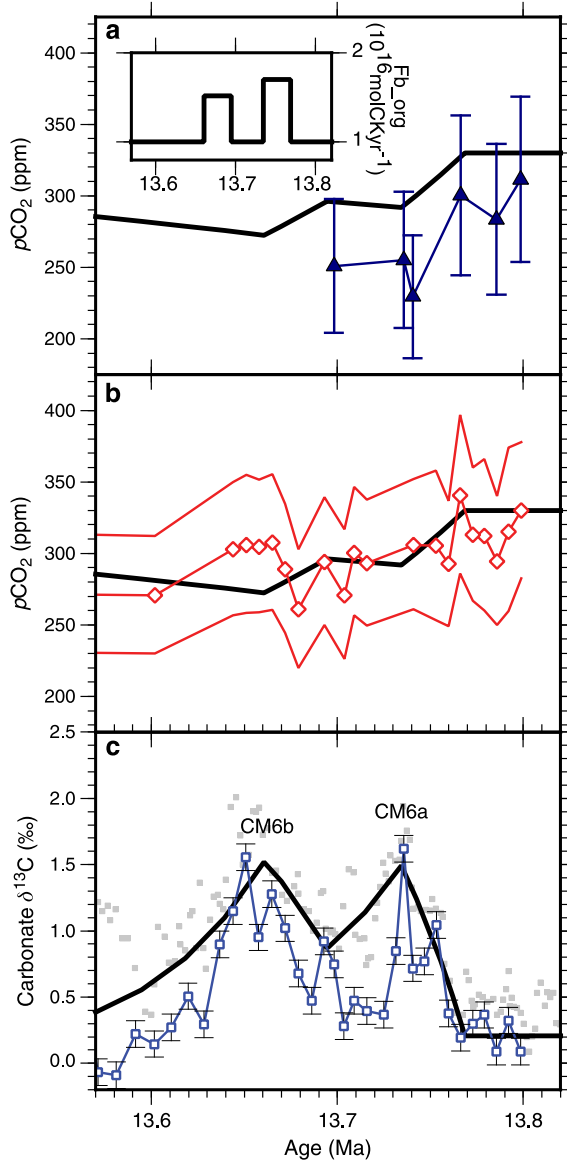
Figure 5. Middle Miocene $p\text{CO}_2$ records. (a) Alkenone $\delta^{13}\text{C}$ based ϵ_p measurements from the Ras il-Pellegrin section (pink open circles with 2σ errors), DSDP Sites 588 (filled black triangles and dotted line) and 608 (filled black squares and dashed line) and ODP Site 730 (gray crosses and solid gray line), [Pagani *et al.*, 1999]. The age model of Pagani *et al.* [1999] has been shifted by -130 kyrs to match our age model, based on the positions of CM6 in the two records. (b) Atmospheric $p\text{CO}_2$ records from alkenone $\delta^{13}\text{C}$ from Ras il-Pellegrin (this study; red open diamonds and solid line with $\pm 2\sigma$ error envelopes) and DSDP Site 588 (dotted line); DSDP Site 608 (dashed line), and ODP Site 730 (solid line) [Pagani *et al.*, 1999], boron isotopes from the Ras il-Pellegrin section (this study; dark blue filled triangles with propagated analytical uncertainties shown as error bars), and ODP Sites 761 (filled black circles) and 926 (open triangles) [Foster *et al.*, 2012], and stomatal indices [Kürschner *et al.*, 2008]. (c) SST record from *G. trilobus* Mg/Ca (black filled circles and line) and alkenone unsaturation index (open circles) from the Ras il-Pellegrin section (this study) and (d) Benthic foraminiferal $\delta^{18}\text{O}$ record from ODP Site 1146 (gray line; [Holbourn *et al.*, 2005]).

changes in North American topography and other boundary conditions in the Miocene prevented glaciation and may have caused a lower $p\text{CO}_2$ threshold for full blown northern hemisphere glaciation to exist during the Miocene [Foster *et al.*, 2010]. Nonetheless, since sea surface temperatures

estimated from both alkenones and *G. trilobus* Mg/Ca ratios at this Mediterranean site indicate temperatures $>29^\circ\text{C}$, our results reaffirm the enigma of a warmer Miocene-world with, at times, less ice than today but only slightly higher levels of atmospheric $p\text{CO}_2$. One potential resolution of

Table 2. Sea surface pH and atmospheric pCO₂ calculated from the maximum and minimum $\delta^{11}\text{B}_{\text{foram}}$ values from our record for a range of assumed $\delta^{11}\text{B}_{\text{SW}}$ calculated assuming total alkalinity = 1300

Assumed Seawater $\delta^{11}\text{B}$ (‰)	Calculated surface pH for $\delta^{11}\text{B}_{\text{foram}} = 16.66$	Calculated surface pH for $\delta^{11}\text{B}_{\text{foram}} = 15.86$	Calculated pCO ₂ for $\delta^{11}\text{B}_{\text{foram}} = 16.66$	Calculated pCO ₂ for $\delta^{11}\text{B}_{\text{foram}} = 15.86$	Calculated CO ₂ change between maximum and minimum $\delta^{11}\text{B}_{\text{foram}}$
36	8.167	8.071	148	196	48
37	8.090	7.987	188	252	64
38	8.005	7.895	242	329	87
39	7.910	7.788	318	444	126
40	7.801	7.660	430	627	197

**Figure 6.** Carbon dioxide reconstructions and modelling. (a) Boron isotope based atmospheric carbon dioxide reconstruction (dark blue filled triangles with propagated analytical uncertainties shown as error bars) and model CO₂ results (black solid line; see text for description); inset: organic matter burial flux model input. (b) Alkenone $\delta^{13}\text{C}$ based pCO₂ reconstruction (red open diamonds and solid line with $\pm 2\sigma$ error envelopes) and model pCO₂ results (black solid line) (c) Fine fraction Ras il-Pellegrin $\delta^{13}\text{C}$ record (blue open squares and line) and modelled average carbonate $\delta^{13}\text{C}$ (black solid line).

these data is that climate sensitivity to pCO₂ is greater than previously thought [Pagani *et al.*, 2010]. The impact of high latitude vegetation on Earth's albedo may have also played an important role in Earth's energy budget in the Miocene [Knorr *et al.*, 2011]. However, further global temperature records are required to solve the Miocene paleoclimate enigma.

[37] **Acknowledgments.** This manuscript is dedicated to the memory of Ben Flower, an inspirational paleoceanographer who will be missed by many. We thank F. J. Hilgen for introducing us to the section, A. A. Mourik for assistance in the field, G. Debono for arranging permissions to work on the section, F. Gill (OGU), J. Becker and J. Green for analytical assistance, P. Pearson for taxonomic assistance and S. Barker for modeling assistance. We also thank Ian D. Bull of the NERC Life Sciences Mass Spectrometry Facility for assistance with alkenone $\delta^{13}\text{C}$ determinations. This manuscript was improved by the careful comments of two anonymous reviewers and the editor. This work was supported by NERC and the National Museum Wales in the form of a CASE studentship (M.P.S.B.), NERC grants NE/D008654/1 and NE/D010241/1 (C.H.L. and R.D.P.), a NERC Advanced Fellowship NERC NE/D00876X/2 (G.L.F.) and NIGL award IP/920/1106 (C.H.L. and R.D.P.).

References

- Abels, H. A., F. J. Hilgen, W. Krijgsman, R. W. Kruk, I. Raffi, E. Turco, and W. J. Zachariasse (2005), Long-period orbital control on middle Miocene global cooling: Integrated stratigraphy and astronomical tuning of the Blue Clay Formation on Malta, *Paleoceanography*, 20, PA4012, doi:10.1029/2004PA001129.
- Allen, K., B. Hönisch, S. M. Eggins, J. Yu, H. J. Spero, H. Elderfield (2011) Controls on boron incorporation in cultured tests of the planktic foraminifer *Orbulina universa*, *Earth Planet. Sci. Lett.*, 309, 291–301, doi:10.1016/j.epsl.2011.07.010.
- Allen, K., and B. Hönisch (2012), The planktic foraminiferal B/Ca proxy for seawater carbonate chemistry: A critical evaluation, *Earth Planet. Sci. Lett.*, 345–348, 203–211, doi:10.1016/j.epsl.2012.06.012.
- Allen, K. A., B. Hönisch, S. M. Eggins, and Y. Rosenthal (2012), Environmental controls on B/Ca in calcite tests of the tropical planktic foraminifer species *Globigerinoides ruber* and *Globigerinoides sacculifer*, *Earth Planet. Sci. Lett.*, 351–352, 270–280, doi:10.1016/j.epsl.2012.07.004.
- Anand, P., H. Elderfield, and M. H. Conte (2003), Calibration of Mg/Ca thermometry in planktonic foraminifera from a sediment trap time series, *Paleoceanography*, 18(2), doi:10.1029/2002PA000846.
- Barker, S., M. Greaves, and H. Elderfield (2003), A study of cleaning procedures used for foraminiferal Mg/Ca paleothermometry, *Geochim. Geophys. Geosyst.*, 4, doi:10.1029/2003GC000559.
- Bellanca, A., F. Sgarrella, R. Neri, B. Russo, M. Sproviera, G. Bonaduce, and D. Rocca (2002), Evolution of the Mediterranean basin during the late Langhian early Serravallian: An integrated paleoceanographic approach, *Riv. Ital. Paleontol. Stratigr.*, 108, 223–239.
- Bidigare, R. R., et al. (1997), Consistent fractionation of C-13 in nature and in the laboratory: Growth-rate effects in some haptophyte algae, *Global Biogeochem. Cycles*, 11, 279–292.
- Bonaduce, G., and D. Barra (2002), The ostracods in the paleoenvironmental interpretation of the late Langhian-early Serravallian Ras il-Pellegrin section (Malta), *Riv. Ital. Paleontol. Stratigr.*, 108, 211–222.
- Catanzaro, E. J., C. E. Champion, E. L. Garner, G. Marinenko, K. M. Sappenfield, and W. R. Shields (1970), Boric assay; isotopic and assay standard reference materials. Institute for Materials Research, National Bureau of Standards, Washington, D.C.
- Coggon, R. M., D. A. H. Teagle, C. E. Smith-Duque, J. C. Alt, and M. J. Cooper (2010), Reconstructing Past Seawater Mg/Ca and Sr/Ca from Mid-Ocean

- Ridge Flank Calcium Carbonate Veins, *Science*, 327(5969), 1114–1117, doi:10.1126/science.1182252.
- Dart, C. J., D. W. J. Bosence, and K. R. McClay (1993), Stratigraphy and Structure of the Maltese Graben System, *J. Geol. Soc.*, 150, 1153–1166.
- DeConto, R. M., D. Pollard, P. A. Wilson, H. Palike, C. H. Lear, and M. Pagani (2008), Thresholds for Cenozoic bipolar glaciation, *Nature*, 455, 652–657, doi:10.1038/nature07337.
- Delaney, M. L., A. W. H. Bé, and E. A. Boyle (1985), Li, Sr, Mg, and Na in foraminiferal calcite shells from laboratory culture, sediment traps, and sediment cores, *Geochim. Cosmochim. Acta*, 49(6), 1327–1341.
- Dickson, A. (1990), Thermodynamics of the dissociation of boric acid in synthetic seawater from 273.15 to 318.15K, *Deep-Sea Res. A. Oceanogr. Rs Pap.*, 37, 755–766.
- Dickson, J. A. D. (2002), Fossil echinoderms as monitor of the Mg/Ca ratio of Phanerozoic oceans, *Science*, 298(5596), 1222–1224, doi:10.1126/science.1075882.
- Dickson, J. A. D. (2004), Echinoderm skeletal preservation: Calcite-aragonite seas and the Mg/Ca ratio of Phanerozoic oceans, *J. Sediment Res.*, 74(3), 355–365, doi:10.1306/112203740355.
- Diester-Haass, L., K. Billups, D. R. Gröcke, L. François, V. Lefebvre, and K. C. Emeis (2009), Mid-Miocene paleoproductivity in the Atlantic Ocean and implications for the global carbon cycle, *Paleoceanography*, 24, PA1209, doi:10.1029/2008PA001605.
- Evans, D., and W. Müller (2012), Deep time foraminifera Mg/Ca palaeothermometry: Nonlinear correction for secular change in seawater Mg/Ca, *Paleoceanography*, 27, PA4205, doi:10.1029/2012PA002315.
- Fantle, M. S., and D. J. DePaolo (2006), Sr isotopes and pore fluid chemistry in carbonate sediment of the Ontong Java Plateau: calcite recrystallization rates and evidence for a rapid rise in seawater Mg over the last 10 million years, *Geochim. Cosmochim. Acta*, 70, 3883–3904, doi:10.1016/j.gca.2006.06.009.
- Fantle, M. S., and D. J. DePaolo (2005), Variations in the marine Ca cycle over the past 20 million years, *Earth Planet. Sci. Lett.*, 237, 102–117, doi:10.1016/j.epsl.2005.06.024.
- Flower, B. P., and J. P. Kennett (1993a), Relations between Monterey Formation Deposition and Middle Miocene Global Cooling - Naples-Beach Section, California, *Geology*, 21, 877–880.
- Flower, B. P., and J. P. Kennett (1993b), Middle Miocene ocean-climate transition: high resolution oxygen and carbon isotopic records from DSDP Site 588A, southwest Pacific, *Paleoceanography*, 8, 811–843.
- Flower, B. P., and J. P. Kennett (1995), Middle Miocene deep water paleoceanography in the southwest Pacific: Relations with East Antarctic ice sheet development, *Paleoceanography*, 10, 1095–1112.
- Foster, G. L. (2008), Seawater pH, pCO₂ and (CO₃²⁻) variations in the Caribbean Sea over the last 130 kyr: A boron isotope and B/Ca study of planktic foraminifera, *Earth Planet. Sci. Lett.*, 271, 254–266, doi:10.1016/j.epsl.2008.04.015.
- Foster, G. L., D. J. Lunt, and R. R. Parrish (2010), Mountain uplift and the glaciation of North America – a sensitivity study, *Climate of the Past*, 6(5), 707–717, doi:10.5194/cp-6-707-2010.
- Foster, G. L., C. H. Lear, and J. W. B. Rae (2012), The evolution of pCO₂, ice volume and climate during the middle Miocene, *Earth Planet. Sci. Lett.*, 341–344, 243–254, doi:10.1016/j.epsl.2012.06.007.
- Hardie, L. A. (1996), Secular variation in seawater chemistry: An explanation for the coupled secular variation in the mineralogies of marine limestones and potash evaporites over the past 600 my, *Geology*, 24(3), 279–283.
- Hasiuk, F. J., and K. C. Lohmann (2010), Application of calcite Mg partitioning functions to the reconstruction of paleocean Mg/Ca, *Geochim. Cosmochim. Acta* 74(23), 6751–6763, doi:10.1016/j.gca.2010.07.030.
- Hemleben, C., M. Spindler, and O. R. Anderson (1989), *Modern Planktonic Foraminifera*, p. 363, Springer-Verlag, New York.
- Hemming, N. G., and G. N. Hanson (1992), Boron isotopic composition and concentration in modern marine carbonates, *Geochim. Cosmochim. Acta*, 56, 537–543.
- Holbourn, A., W. Kuhnt, M. Schulz, and H. Erlenkeuser (2005), Impacts of orbital forcing and atmospheric carbon dioxide on Miocene ice-sheet expansion, *Nature*, 438, 483–487, doi:10.1038/nature04123.
- Holbourn, A., W. Kuhnt, M. Schulz, and J. Flores (2007), Orbitally-paced climate evolution during the middle Miocene “Monterey” carbon-isotope excursion, *Earth Planet. Sci. Lett.*, 261, 534–550, doi:10.1016/j.epsl.2007.07.026.
- Hollander, D. J., and J. A. McKenzie (1991), CO₂ control on carbon-isotope fractionation during aqueous photosynthesis - a paleo-pCO₂ barometer, *Geology*, 19, 929–932.
- Horita, J., H. Zimmermann, and H. D. Holland (2002), Chemical evolution of seawater during the Phanerozoic: Implications from the record of marine evaporites, *Geochim. Cosmochim. Acta*, 66, 3733–3756, doi:10.1016/S0016-7037(01)00884-5.
- Huguet, C., J.-H. Kim, G. J. de Lange, J. S. Sinninghe Damste, and S. Schouten (2009), Effects of long term oxic degradation on the U₅⁷, TEX₈₆ and BIT organic proxies, *Org. Geochem.*, 40, 1188–1194, doi:10.1016/j.orggeochem.2009.09.003.
- Jasper, J. P., J. M. Hayes, A. C. Mix, and F. G. Prahl (1994), Photosynthetic fractionation of ¹³C and concentrations of dissolved CO₂ in the central equatorial Pacific during the last 255,000 years, *Paleoceanography*, 9, 781–798.
- Knorr, G., M. Butzin, M. A. Micheels, and G. Lohmann (2011), A warm Miocene climate at low atmospheric CO₂ levels, *Geophys. Res. Lett.*, 38, L20701, doi:10.1029/2011GL048873.
- Kump, L. R., and M. A. Arthur (1999), Interpreting carbon-isotope excursions: carbonates and organic matter, *Chem. Geol.*, 161, 181–198.
- Klochko, K., A. J. Kaufman, W. S. Yao, R. H. Byrne, and J. A. Tossell (2006), Experimental measurement of boron isotope fractionation in seawater, *Earth Planet. Sci. Lett.*, 248(1–2), 276–285, doi:10.1016/j.epsl.2006.05.034.
- Klochko, K., G. D., Tossell, J. A., Dera, P., and Kaufman, A. J. (2009), Re-evaluating boron speciation in biogenic calcite and aragonite using ¹¹B MAS NMR, *Geochim. Cosmochim. Acta*, 73, 1890–1900, doi:10.1016/j.gca.2009.01.002.
- Kürschner, W. M., Z. Kvaček, and D. L. Dilcher (2008), The impact of Miocene atmospheric carbon dioxide fluctuations on climate and the evolution of terrestrial ecosystems, *Proc. Natl. Acad. Sci. U.S.A.*, 105, 449–453, doi:10.1073/pnas.0708588105.
- Laws, E. A., B. N. Popp, R. R. Bidigare, M. C. Kennicutt, and S. A. Macko (1995), Dependence of phytoplankton carbon isotope composition on growth rate and [CO₂]_{aq}: Theoretical considerations and experimental results, *Geochim. Cosmochim. Acta*, 59, 1131–1138.
- Lear, C. H., H. Elderfield, and P. A. Wilson (2000), Cenozoic deep-sea temperatures and global ice volumes from Mg/Ca in benthic foraminiferal calcite, *Science*, 287, 269–272.
- Lear, C. H., Y. Rosenthal, H. K. Coxall, and P. A. Wilson (2004), Late Eocene to early Miocene ice sheet dynamics and the global carbon cycle, *Paleoceanography*, 19, PA4015, doi:10.1029/2004PA001039.
- Lemarchand, D., J. Gaillardet, E. Lewin, and C. J. Allègre (2002), Boron isotope systematics in large rivers: Implications for the marine boron budget and paleo-pH reconstruction over the Cenozoic, *Chem. Geol.*, 190, 123–140, doi:10.1016/S0009-2541(02)00114-6.
- Lowenstein, T. K., M. N. Timofeeff, S. T. Brennan, L. A. Hardie, and R. V. Demicco (2001), Oscillations in Phanerozoic seawater chemistry: Evidence from fluid inclusions, *Science*, 294(5544), 1086–1088, doi:10.1126/science.1064280.
- Marlowe, I. T., S. C. Brassell, G. Eglinton, and J. C. Green (1990), Long-chain alkenones and alkyl alkenoates and the fossil coccolith record of marine sediments, *Chem. Geol.*, 88, 349–375.
- Maslin, M. A., N. J. Shackleton, and U. Pflaumann (1995), Surface-Water Temperature, Salinity, and Density Changes in the Northeast Atlantic during the Last 45,000 Years - Heinrich Events, Deep-Water Formation, and Climatic Rebounds, *Paleoceanography* 10, 527–544.
- Miller, K. G., J. D. Wright, and R. G. Fairbanks (1991), Unlocking the ice house: Oligocene-Miocene oxygen isotopes, eustasy and margin erosion, *J. Geophys. Res.*, 96, 6829–6848.
- Mourik, A. A., H. A. Abels, F. J. Hilgen, A. Di Stefano, and W. J. Zachariasse (2011), Improved astronomical age constraints for the Middle Miocene Climate Transition based on high-resolution stable isotope records from the central Mediterranean Maltese Islands, *Paleoceanography*, 26, PA1210, doi:10.1029/2010PA001981.
- Müller, P. J., G. Kirst, G. Ruhland, I. von Storch, and A. Rosell-Mele (1998), A calibration of the alkenone paleotemperature index U₃₇(K') based on core-tops from the eastern South Atlantic and the global ocean (60 degrees N–60 degrees S), *Geochim. Cosmochim. Acta*, 62, 1757–1772.
- Ni, Y. Y., G. L. Foster, T. R. Bailey, T. Elliott, D. N. Schmidt, P. Pearson, B. Haley, and C. Coath (2007), A core top assessment of proxies for the ocean carbonate system in surface-dwelling foraminifers, *Paleoceanography*, 3, doi:PA3212/0002489009000001.
- Pagani, M., M. A. Arthur, and K. H. Freeman (1999), Miocene evolution of atmospheric carbon dioxide, *Paleoceanography*, 14, 273–292.
- Pagani, M., J. C. Zachos, K. H. Freeman, B. Tipple, and S. Bohaty (2005), Marked decline in atmospheric carbon dioxide concentrations during the Paleogene, *Science*, 309, 600–603, doi:10.1126/science.1110063.
- Pagani, M., Z. Liu, J. LaRivière, and A. C. Ravelo (2010), High Earth-system climate sensitivity determined from Pliocene carbon dioxide concentrations, *Nature Geosci.*, 3, 29–30 doi:10.1038/NGEO724.
- Paris, G., J. Gaillardet, and P. Louvat (2010), Geological evolution of seawater boron isotopic composition recorded in evaporate, *Geology*, 38, 1035–1038, doi:10.1130/G31321.11.
- Pearson, P. N., P. W. Ditchfield, J. Singano, K. G. Harcourt-Brown, C. J. Nicholas, R. K. Olsson, N. J. Shackleton, and M. A. Hall (2001), Warm tropical sea surface temperatures in the Late Cretaceous and Eocene epochs, *Nature*, 413, 481–487, doi:10.1038/35097000.
- Pearson, P. N., and M. R. Palmer (2000), Atmospheric carbon dioxide concentrations over the past 60 million years, *Nature*, 406, 695–699, doi:10.1038/35021000.

- Popp, B. N., E. A. Laws, R. R. Bidigare, J. E. Dore, K. L. Hanson, and S. G. Wakeham (1998a), Effect of phytoplankton cell geometry on carbon isotopic fractionation, *Geochim. Cosmochim. Acta*, 62, 69–77.
- Popp, B. N., F. Kenig, S. G. Wakeham, E. A. Laws, and R. R. Bidigare (1998b), Does growth rate affect ketone unsaturation and intracellular carbon isotopic variability in *Emiliana huxleyi*?, *Paleoceanography*, 13, 35–41.
- Rae, J. W. B., G. L. Foster, D. N. Schmidt, and T. Elliot (2011), Boron isotopes and B/Ca in benthic foraminifera: proxies for the deep ocean carbonate system. *Earth Planet. Sci. Lett.*, 302, 403–413, doi:10.1016/j.epsl.2010.12.034.
- Sanyal, A., J. Bijma, H. Spero, and D. W. Lea (2001), Empirical relationship between pH and boron isotopic composition of *Globigerinoides sacculifer*: Implications for the boron isotope paleo-pH proxy, *Paleoceanography*, 16, 515–519.
- Seki, O., G. L. Foster, D. N. Schmidt, A. Mackensen, K. K. Kawamure, and R. D. Pancost (2010), Alkenone and boron based Plio-Pleistocene pCO₂ records, *Earth Planet. Sci. Lett.*, 292, 201–211, doi:10.1016/j.epsl.2010.01.037.
- Shevenell, A. E., J. P. Kennett, and D. W. Lea (2008), Middle Miocene ice sheet dynamics, deep-sea temperatures, and carbon cycling: A Southern Ocean perspective, *Geochem. Geophys. Geosyst.*, 9, Q02006, doi:10.1029/2007GC001736.
- Simon, L., C. Lécuyer, C. Maréchal, and N. Coltice (2006), Modelling the geochemical cycle of boron: Implications for the long-term delta B-11 evolution of seawater and oceanic crust, *Chem. Geol.*, 225, 61–76, doi:10.1016/j.chemgeo.2005.08.011.
- Tian J., A. Shevenell, P. Wang, Q. Zhao, Q. Li, and X. Cheng (2009), Reorganization of Pacific Deep Waters linked to middle Miocene Antarctic cryosphere expansion: A perspective from the South China Sea, *Palaeogeogr., Palaeoclimatol., Palaeoecol.*, 284(3–4), 375–382, doi:10.1016/j.palaeo.2009.10.019.
- Tyrrell, T., and R. E. Zeebe (2004), History of carbonate ion concentration over the last 100 million years, *Geochim. Cosmochim. Acta*, 68(17), 3521–3530, doi:10.1016/j.gca.2004.02.018.
- Vincent, E., and W. H. Berger (1985), Carbon dioxide and polar cooling in the Miocene: the Monterey hypothesis, in *The carbon cycle and atmospheric CO₂: natural variations Archean to present. Chapman conference papers*, 1984, 455–468.
- Wilkinson, B. H., and T. J. Algeo (1989), Sedimentary carbonate record of calcium-magnesium cycling. *Am. J. Sci.*, 289, 1158–1194.
- Woodruff, F., and S. Savin (1991), Mid-Miocene isotope stratigraphy in the deep sea: high resolution correlations, paleoclimatic cycles, and sediment preservation, *Paleoceanography*, 6, 755–806.
- Yu, J. M., H. Elderfield, and B. Honisch (2007), B/Ca in planktonic foraminifera as a proxy for surface seawater pH, *Paleoceanography*, 22(2), doi:10.1029/2006PA001347.
- Zachos, J., M. Pagani, L. Sloan, E. Thomas, and K. Billups (2001), Trends, rhythms, and aberrations in global climate 65 Ma to present, *Science*, 292, 686–693, doi:10.1126/science.1059412.
- Zeebe, R. E., and D. Wolf-Gladrow (2001), CO₂, in *Seawater: Equilibrium, Kinetics, Isotopes*, Elsevier Oceanography Series, vol. 65, Elsevier, Amsterdam.